Springer

Available online at https://link.springer.com/journal/42241
http://www.jhydrodynamics.com
Journal of Hydrodynamics, 2020, 32(6): 1191-1206
https://doi.org/10.1007/s42241-019-0076-3

Reduction of wave impact on seashore as well as seawall by floating structure and bottom topography *

Amandeep Kaur, S. C. Martha
Department of Mathematics, Indian Institute of Technology Ropar, Rupnagar, Punjab, India

(Received December 24, 2018, Revised June 13, 2019, Accepted June 21, 2019, Published online October 12, 2019)

Abstract: The three-dimensional problem involving diffraction of water wave by a finite floating rigid dock over an arbitrary bottom is studied for two cases (1) in the absence of wall (2) in the presence of wall. The problem is handled for its solution with the aid of step method. Here both asymmetric and symmetric arbitrary bottom profile is approximated using successive steps. Step approximation helps to apply the matched eigenfunction expansion method, in result, system of algebraic equations are obtained which are solved to determine the hydrodynamic quantities, namely, force experienced by rigid floating dock as well as rigid seawall, free surface elevation, transmission and reflection coefficients associated with transmission and reflected waves respectively. The effects of various structural and system parameters are examined on these hydrodynamics quantities. The appropriate values of length and thickness of dock, water depth and angle of incidence provide the salient information to marine and coastal engineers to design the offshore structures and creation of parabolic trench on the bottom. The present results are compared with known results in special case of bottom topography. The energy balance relation is derived and checked.

Key words: Arbitrary bottom, step approximation, hydrodynamic quantities

Introduction

The floating structures having different geometries have been studied due to their significant applications in the field of coastal and ocean engineering. For instance, floating structures are used to implement various marine and coastal management activities such as wave energy device, breakwater, offshore platforms (for oil recovery), ship navigation and sea shore protection etc.. The problems involving scattering of surface waves by floating rigid dock over finite or infinite depth of water have been studied by many researchers using different solution techniques (see Linton[1], Chakrabarti et al.[2] and the references therein). The interaction of oblique incident waves with a horizontal flexible membrane, in finite depth of water was investigated by Cho and Kim[3] and they found that a properly designed horizontal flexible membrane can be an effective wave barrier. These structures are constructed along the shoreline with the assumption that seabed is of uniform flat type. But it is often difficult to find flat bed around the shoreline, hence sudden change in the bottom topography needs to be considered which plays significant role in designing and construction of coastal structures. In this context, the problems of wave scattering in the presence of a small undulation on seabed have been studied by many researchers: Martha and Bora[4] and many others. They used the perturbation technique due to the smallness of the bottom undulations. When the undulation is not small, such problems can be handled using mild-slope approximation[5]. Further, the problem involving linear long-wave reflection by an obstacle of general trapezoidal shape was explored by Lin and Liu[6]. They found the closed-form expression in terms of first and second kinds of Bessel functions for the wave reflection coefficient. The problem of linear long-wave reflection by a rectangular obstacle with two scour trenches has been explored by Xie et al.[7]. They found that zero reflection exists for a rectangular obstacle as long as the bathymetry is symmetrical. Moreover, Wang and Meylan[8] used boundary element method to study the problem involving scattering phenomenon of water waves by a floating thin elastic plate over variable depth of water. Xu and Lu[9] provided a method involving an optimization of eigenfunction expansion

* **Biography:** Amandeep Kaur, Ph. D. Candidate,
E-mail: amandeep.kaur@iitrpr.ac.in
Corresponding author: S. C. Martha,
E-mail: scmartha@gmail.com

to study the problem of water wave interaction with a semi-infinite elastic plate.

Further, the problems of wave structure interaction over step type bottom topography have been studied by many researchers. For example, Karmakar and Sahoo[10] studied the problem of water wave scattering for two cases (1) semi-infinite membrane, (2) finite floating membrane in the presence of single step of finite depth. They also considered the case of infinite depth. Dhillon et al.[11] studied the problem of surface water wave interaction with a rigid thin dock in the presence of a single stepped bottom topography using matched eigenfunction expansion method. The problem of wave scattering by a semi elastic plate in the presence of step was studied by Guo et al.[12]. The problem of diffraction of obliquely incident water waves by a vertical porous structure placed over stepped bottom topography was studied by Das and Bora[13]. Meng and Lu[14] investigated the reflection and transmission coefficients for scattering of free-surface gravity wave by a porous rectangular barrier mounted on seabed by using inner product method. In the recent experimental study by Zhao et al.[15], it is found that the surface elevation at the front face of an offshore structure can reach up to four times the incident wave amplitude even in random sea state. Based on the above studies, to protect the seashore, it is important to consider the problem involving diffraction of obliquely incident water waves by thick floating structure over arbitrary bottom, which have been studied in this paper.

Moreover, it has been seen that the rigid vertical seawall is constructed near the shoreline to protect the back-land. In some locations, potential hazard happens due to shore erosion, for example, the road or buildings near the shoreline are about to fall into water due to shore erosion. Hence, the construction of seawall provides an alternative approach for coastal protection. Further, it may be noted that due to high wave impact, the sea wall may collapse. These high waves will not only affect the seawall but also move the sand away from the base of the seawall. Hence, the structural safety and stability of the seawall should be considered while designing the offshore structures. In this direction, Liu et al.[16] studied the problem of wave interaction with a perforated breakwater for reduction of wave reflection and wave force on seawall. Further, they studied the problem involving interaction between obliquely incident waves and an infinite array of multi-chamber perforated caissons and developed an analytical solution by using matched eigenfunction expansion method[17]. The problem of wave trapping by different structures over flat or step type bottom has been studied by many authors. For example, Bhattacharjee and Soares[18] studied the problem of wave-structure interaction in the presence of wall over a single step bottom topography using matched eigenfunction expansion method. The problem of wave trapping by porous barrier in the presence of step type bottom is examined by Behera et al.[19] by using modified mild-slope equation and eigenfunction expansion method. Further, the problem of wave trapping by permeable membrane located near a wall was studied by Koley et al.[20]. In most of these studies, the seawall is protected by considering thin vertical structure over flat bed or step type bottom. Hence, by placing a floating structure at a finite distance from the seawall and constructing submarine parabolic trench at the bottom bed, will create a calm zone by reducing the transmission of wave energy and this will provide an alternate solution in reduction of high wave impact on seawall as well as on seashore. To the authors' knowledge, the literature related to thick rigid floating structure over arbitrary bottom is very limited. In the present paper, we have made an effort to study the way to protect sea shore and/or seawall by placing a rigid floating thick structure over an arbitrary bottom. The arbitrary bottom asymmetric or symmetric in nature can be approximated by successive flat shelves by which the method of eigenfunction expansion is well applicable (rather than applying a numerical method). This process yields a system of equations which is solved to determine the numerical values of transmission and reflection coefficients associated with the original boundary value problem for a few arbitrary profiles such as parabolic, triangular, trapezoidal and rectangular bottom. In addition to this, free surface elevation profiles, vertical and horizontal components of the force experienced by the floating rigid dock as well as rigid wall are examined for various values of structural and system parameters in the case of arbitrary bottom, especially for the parabolic profile. Present results are validated by comparing with the known results, which reveals an excellent agreement with the results for particular case of bottom topography. The energy identity is derived and verified.

1. Mathematical formulation of the problem

The three-dimensional problem of water wave interaction with a floating rigid dock over arbitrary bottom topography is considered for two cases: (1) in the absence of wall, (2) in the presence of wall. The dock situated at the free surface has finite length and thickness. The arbitrary bottom topography is approximated by a series of steps. Here y-axis is chosen vertically downward and xy-horizontal plane is taken to be an undisturbed free surface of water in the Cartesian coordinate system.

1.1 *In the absence of wall*

It is assumed that the floating rigid dock has length $2l$ and thickness d and it is situated at the free surface with position $y=0$, $-l\le x\le l$ It is assumed that the floating structure is infinitely long in the z - direction and hence the characteristic behavior remains the same in the z - direction. Here, an asymmetric arbitrary bottom topography is taken (see Fig. 1) and is described by $y=H(x)$, where $H(x)=h(x)$, $-a\le x\le a$ with $a<l$ and $H(x)=h_0$, $x\le -a$ and $H(x)=\hat{h}_0$, $x\ge a$.

It should be noted that the water depths before and after the uneven bottom are not equal. In particular, equal depth i.e., symmetric shape is also considered to examine the problem. Here, the uneven shape is approximated by a series of steps for which m number of steps are considered in downward direction and m number of steps is considered in upward direction. Note that one may take different number of steps in both directions. Hence, m shelves given by $-a_i\le x\le -a_{i-1}$ with depth $h_{(m+1)-i}$, $i=1,2,\cdots,m$ are created in $-a\le x\le 0$ and m shelves given by $a_{i-1}\le x\le a_i$ with depth h_{m+i}, $i=1,2,\cdots,m$ are created in $0\le x\le a$. So, there are m steps at $x=-a_i$, $i=1,2,\cdots,m$ the interval $[-a,0]$ and m steps at $x=a_i$, $i=1,2,\cdots,m$ in the interval $[0,a]$. The whole domain of fluid is divided into $2m+4$ regions where region R_1 is $\{-\infty\le x\le -l$, $0\le y\le h_0\}$ region R_2 is $\{-l\le x\le -a_m$, $d\le y\le h_0\}$, regions $R_j\,(j=3,4,\cdots,m+2)$ are $\{-a_{m+3-j}\le x\le -a_{m+2-j}$, $d\le y\le h_{j-2}\}$, regions $R_j\,(j=m+3,m+4,\cdots,2m+2)$ are $\{a_{j-(m+3)}\le x\le a_{j-(m+2)}$, $d\le y\le h_{j-2}\}$, $j=m+3,m+4,\cdots,2m+2$ and region R_{2m+3} is $\{a_m\le x\le l$, $d\le y\le \hat{h}_0\}$ and the last region R_{2m+4} is $\{l\le x\le\infty$, $0\le y\le \hat{h}_0\}$as shown in Fig. 1. In the figure, it is assumed that: $h_i\le h_{i+1}$, $i=0,1,\cdots,m-1$, $h_i=h_{i+1}$, $i=m$, $h_i\ge h_{i+1}$, $i=m+1,m+2,\cdots,2m-1$ and $h_{2m}\ge\hat{h}_0$. For an incompressible and irrotational fluid motion which is simple harmonic in time t, then in each region R_j, the fluid motion can be characterized by the velocity potential $\Phi_j(x,y,z,t)=Re[\phi_j(x,y)\mathrm{e}^{-\mathrm{i}\omega t+\mathrm{i}\upsilon z}]$, $j=1,2,\cdots,2m+4$ with angular frequency ω, angle of incidence θ and $\upsilon=k_0\sin\theta$ (υ is the z component of the wave number k_0 associated with the incident wave) and $\phi^{inc}(x,y,z,t)=Re\{[\cosh k_0(y-h_0)/\cosh k_0h_0]\mathrm{e}^{\mathrm{i}k_{0x}x-\mathrm{i}\omega t+\mathrm{i}\upsilon z}\}$, where $k_{0x}=k_0\cos\theta=+\sqrt{k_0^2-\upsilon^2}$ (x component of the wave number k_0 associated with the incident wave) and k_0 is the unique positive root of $k\tanh kh_0-K=0$ and $\phi_j(x,y)$ satisfies

$$\frac{\partial^2\phi_j}{\partial x^2}+\frac{\partial^2\phi_j}{\partial y^2}-\upsilon^2\phi_j=0 \tag{1}$$

in each fluid region R_j, where $j=1,2,\cdots,2m+4$.

The linearized condition in the open water region can be obtained as:

$$\frac{\partial\phi_j}{\partial y}+K\phi_j=0 \quad \text{on} \quad y=0,\ |x|\ge l \tag{2a}$$

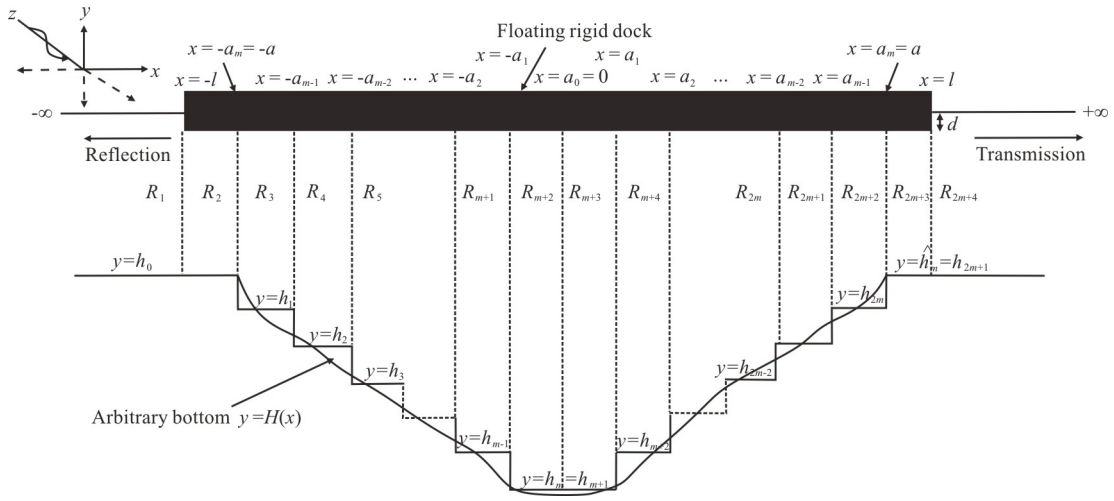

Fig. 1 Schematic of physical problem

$$\frac{\partial \phi_j}{\partial y} + K\phi_j = 0 \quad \text{on} \quad j = 1, 2m+4 \tag{2b}$$

Here, $K = \omega^2 / g$ and g is an acceleration due to gravity.

In region R_1, ϕ_1 satisfies the following boundary conditions:

$$\frac{\partial \phi_1}{\partial y} = 0 \quad \text{on} \quad y = h_0, \quad x \le -l \tag{3}$$

$$\frac{\partial \phi_1}{\partial x} = 0 \quad \text{on} \quad x = -l, \quad 0 \le y \le d \tag{4}$$

In region R_2, ϕ_2 satisfies following boundary conditions:

$$\frac{\partial \phi_2}{\partial y} = 0 \quad \text{on} \quad y = d, \quad y = h_0 \tag{5a}$$

$$\frac{\partial \phi_2}{\partial y} = 0 \quad \text{on} \quad -l \le x \le -a_m \tag{5b}$$

In region R_j where $j = 3, 4, \cdots, m+2$, ϕ_j satisfies following boundary conditions:

$$\frac{\partial \phi_j}{\partial y} = 0 \quad \text{on} \quad y = d, \quad y = h_{j-2} \tag{6a}$$

$$\frac{\partial \phi_j}{\partial y} = 0 \quad \text{on} \quad -a_{m+3-j} \le x \le -a_{m+2-j} \tag{6b}$$

$$\frac{\partial \phi_j}{\partial x} = 0 \quad \text{on} \quad x = -a_{m+3-j} \tag{7a}$$

$$\frac{\partial \phi_j}{\partial x} = 0 \quad \text{on} \quad h_{j-3} \le y \le h_{j-2.} \tag{7b}$$

In region R_j where $j = m+3, m+4, \cdots, 2m+2$, ϕ_j satisfies following boundary conditions:

$$\frac{\partial \phi_j}{\partial y} = 0 \quad \text{on} \quad y = d, \quad y = h_{j-2} \tag{8a}$$

$$\frac{\partial \phi_j}{\partial y} = 0 \quad \text{on} \quad a_{j-(m+3)} \le x \le a_{j-(m+2)} \tag{8b}$$

$$\frac{\partial \phi_j}{\partial x} = 0 \quad \text{on} \quad x = a_{j-(m+2)} \tag{9a}$$

$$\frac{\partial \phi_j}{\partial x} = 0 \quad \text{on} \quad h_{j-1} \le y \le h_{j-2} \tag{9b}$$

with $\hat{h}_0 = h_{2m+1}$.

In region R_{2m+3}, ϕ_{2m+3} satisfies following boundary conditions:

$$\frac{\partial \phi_{2m+3}}{\partial y} = 0 \quad \text{on} \quad y = d, \quad y = \hat{h}_0 \tag{10a}$$

$$\frac{\partial \phi_{2m+3}}{\partial y} = 0 \quad \text{on} \quad a_m \le x \le l \tag{10b}$$

In region R_{2m+4}, ϕ_{2m+4} satisfies the boundary conditions:

$$\frac{\partial \phi_{2m+4}}{\partial y} = 0 \quad \text{on} \quad y = \hat{h}_0, \quad x \ge l \tag{11}$$

$$\frac{\partial \phi_{2m+4}}{\partial x} = 0 \quad \text{on} \quad x = l, \quad 0 \le y \le d \tag{12}$$

Due to the scattering of surface water waves, $\phi_1(x, y)$ and $\phi_{2m+4}(x, y)$, respectively in regions R_1 and R_{2m+4} satisfy the conditions:

$$\phi_1(x, y) \to [e^{ik_{0x}(x+l)} + Re^{-ik_{0x}(x+l)}] f_0(y) \quad \text{as} \quad x \to -\infty \tag{13}$$

$$\phi_{2m+4}(x, y) \to Te^{ip_{0x}(x-l)} g_0(y) \quad \text{as} \quad x \to \infty \tag{14}$$

where $p_{0x} = +\sqrt{p_0^2 - \upsilon^2}$ and p_0 is the unique positive root of $p \tanh p\hat{h}_0 = K$. R and T are the unknown complex constants associated with the amplitude of reflected and transmitted waves respectively.

1.2 *Method of solution*

The method of matching eigenfunction expansion is utilized to solve the associated mixed boundary value problem involving Eqs. (1)-(14). Havelock's expansion of the velocity potential ϕ_j ($j = 1, 2, \cdots, 2m+4$) in each region R_j is given by:

$$\phi_1(x, y) = [e^{ik_{0x}(x+l)} + Re^{-ik_{0x}(x+l)}] f_0(y) + \sum_{n=1}^{\infty} A_n e^{k_{nx}(x+l)} f_n(y), \quad -\infty < x \le -l, \quad 0 < y < h_0 \tag{15}$$

$$\phi_2(x,y)=B_{0,2}\mathrm{e}^{\mathrm{i}\alpha_{0x}^{(2)}x}+C_{0,2}\mathrm{e}^{-\mathrm{i}\alpha_{0x}^{(2)}x}+$$

$$\sum_{n=1}^{\infty}[B_{n,2}\mathrm{e}^{\alpha_{nx}^{(2)}x}+C_{n,2}\mathrm{e}^{-\alpha_{nx}^{(2)}x}]\psi_{n,2}(y),$$

$$-l<x\le -a_m,\quad d<y<h_0 \tag{16}$$

$$\phi_j(x,y)=B_{0,j}\mathrm{e}^{\mathrm{i}\alpha_{0x}^{(j)}x}+C_{0,j}\mathrm{e}^{-\mathrm{i}\alpha_{0x}^{(j)}x}+$$

$$\sum_{n=1}^{\infty}[B_{n,j}\mathrm{e}^{\alpha_{nx}^{(j)}x}+C_{n,j}\mathrm{e}^{-\alpha_{nx}^{(j)}x}]\psi_{n,j}(y),$$

$$j=3,4,\cdots,m+2,\quad -a_{m+3-j}\le x\le -a_{m+2-j},$$

$$d<y<h_{j-2} \tag{17}$$

$$\phi_j(x,y)=B_{0,j}\mathrm{e}^{\mathrm{i}\alpha_{0x}^{(j)}x}+C_{0,j}\mathrm{e}^{-\mathrm{i}\alpha_{0x}^{(j)}x}+$$

$$\sum_{n=1}^{\infty}[B_{n,j}\mathrm{e}^{\alpha_{nx}^{(j)}x}+C_{n,j}\mathrm{e}^{-\alpha_{nx}^{(j)}x}]\psi_{n,j}(y),$$

$$j=m+3,m+4,\cdots,2m+2,$$

$$a_{j-(m+3)}\le x\le a_{j-(m+2)},\quad d<y<h_{j-2} \tag{18}$$

$$\phi_j(x,y)=B_{0,j}\mathrm{e}^{\mathrm{i}\alpha_{0x}^{(j)}x}+C_{0,j}\mathrm{e}^{-\mathrm{i}\alpha_{0x}^{(j)}x}+$$

$$\sum_{n=1}^{\infty}[B_{n,j}\mathrm{e}^{\alpha_{nx}^{(j)}x}+C_{n,j}\mathrm{e}^{-\alpha_{nx}^{(j)}x}]\psi_{n,j}(y),$$

$$j=2m+3,\quad a_m\le x\le l,\quad d\le y<\hat{h}_0 \tag{19}$$

$$\phi_{2m+4}(x,y)=T\mathrm{e}^{\mathrm{i}p_{0x}(x-l)}g_0(y)+\sum_{n=1}^{\infty}D_n\mathrm{e}^{-p_{nx}(x-l)}g_n(y),$$

$$l\le x\le\infty,\quad 0<y<\hat{h}_0 \tag{20}$$

Here, R, T, A_n, $B_{0,j}$, $C_{0,j}$, $B_{n,j}$, $C_{n,j}$, D_n, $j=2,3,\cdots,2m+3$, $n=1,2,\cdots$ are unknown complex constants be determined k_n and $p_n\,(n=1,2,\cdots)$ are the roots of $k\tan kh_0=-K$ and $p\tan p\hat{h}_0=-K$ respectively and $k_{nx}=+\sqrt{k_n^2+\upsilon^2}$, $p_{nx}=+\sqrt{p_n^2+\upsilon^2}$, $n=1,2,\cdots$, $\alpha_{nx}^{(j)}=+\sqrt{[\alpha_n^{(j)}]^2+\upsilon^2}$, $j=2,3,\cdots,2m+3$, $n=0,1,2,\cdots$ and

$$f_0(y)=\frac{\cosh k_0(y-h_0)}{\cosh k_0h_0} \tag{21}$$

$$f_n(y)=\frac{\cos k_n(y-h_0)}{\cos k_nh_0},\quad n=1,2,\cdots \tag{22}$$

$$\psi_{n,j}(y)=\frac{\cos\alpha_n^{(j)}(y-h_{j-2})}{\cos\alpha_n^{(j)}h_{j-2}},\quad n=0,1,2,\cdots,$$

$$j=2,3,\cdots,2m+3 \tag{23}$$

$$\alpha_n^{(j)}=\frac{n\pi}{h_{j-2}-d},\quad j=2,3,\cdots,2m+3,\quad n=0,1,2,\cdots \tag{24}$$

$$g_0(y)=\frac{\cosh p_0(y-\hat{h}_0)}{\cosh p_0\hat{h}_0} \tag{25}$$

$$g_n(y)=\frac{\cos p_n(y-\hat{h}_0)}{\cos p_n\hat{h}_0},\quad n=1,2,\cdots \tag{26}$$

For the case of normal incidence i.e., $\theta=0°$ implies $\upsilon=0$ the expansion for velocity potential ϕ_j, $j=2,3,\cdots,2m+3$ in respective regions take the following form:

$$\phi_2(x,y)=B_{0,2}+C_{0,2}\frac{x}{l}+$$

$$\sum_{n=1}^{\infty}[B_{n,2}\mathrm{e}^{\alpha_{nx}^{(2)}x}+C_{n,2}\mathrm{e}^{-\alpha_{nx}^{(2)}x}]\psi_{n,2}(y),$$

$$-l<x\le -a_m,\quad d<y<h_0 \tag{27}$$

$$\phi_j(x,y)=B_{0,j}+C_{0,j}\frac{x}{a_{m+3-j}}+$$

$$\sum_{n=1}^{\infty}[B_{n,j}\mathrm{e}^{\alpha_{nx}^{(j)}x}+C_{n,j}\mathrm{e}^{-\alpha_{nx}^{(j)}x}]\psi_{n,j}(y),$$

$$j=3,4,\cdots,m+2,\quad -a_{m+3-j}\le x\le -a_{m+2-j},$$

$$d<y<h_{j-2} \tag{28}$$

$$\phi_j(x,y)=B_{0,j}+C_{0,j}\frac{x}{a_{j-(m+2)}}+$$

$$\sum_{n=1}^{\infty}[B_{n,j}\mathrm{e}^{\alpha_{nx}^{(j)}x}+C_{n,j}\mathrm{e}^{-\alpha_{nx}^{(j)}x}]\psi_{n,j}(y),$$

$j=m+3,m+4,\cdots,2m+2$,

$a_{j-(m+3)}\le x\le a_{j-(m+2)}$, $d<y<h_{j-2}$ (29)

$$\phi_j(x,y)=B_{0,j}+C_{0,j}\frac{x}{l}+$$

$$\sum_{n=1}^{\infty}[B_{n,j}\mathrm{e}^{\alpha_{nx}^{(j)}x}+C_{n,j}\mathrm{e}^{-\alpha_{nx}^{(j)}x}]\psi_{n,j}(y),$$

$j=2m+3$, $a_m\le x\le l$, $d\le y<\hat{h}_0$ (30)

The continuity of pressure and velocity at $x=-l$ gives:

$\phi_1(-l_-,y)=\phi_2(-l_+,y)$, $d<y<h_0$ (31a)

$\phi_{1x}(-l_-,y)=\phi_{2x}(-l_+,y)$, $d<y<h_0$ (31b)

The continuity of pressure and velocity at $x=-a_{m+2-j}$, $j=2,3,\cdots,m+2$ gives:

$\phi_j(-a_{m+2-j_-},y)=\phi_{j+1}(-a_{m+2-j_+},y)$, $d<y<h_{j-2}$ (32a)

$\phi_{jx}(-a_{m+2-j_-},y)=\phi_{(j+1)x}(-a_{m+2-j_+},y)$, $d<y<h_{j-2}$ (32b)

The continuity of pressure and velocity at $x=a_{j-(m+2)}$, $j=m+3,m+4\cdots,2m+2$ gives:

$\phi_j(a_{j-(m+2)_-},y)=\phi_{j+1}(a_{j-(m+2)_+},y)$, $d<y<h_{j-1}$ (33a)

$\phi_{jx}(a_{j-(m+2)_-},y)=\phi_{(j+1)x}(a_{j-(m+2)_+},y)$, $d<y<h_{j-1}$ (33b)

The continuity of pressure and velocity at $x=l$ gives:

$\phi_{2m+3}(l_-,y)=\phi_{2m+4}(l_+,y)$, $d<y<\hat{h}_0$ (34a)

$\phi_{(2m+3)x}(l_-,y)=\phi_{(2m+4)x}(l_+,y)$, $d<y<\hat{h}_0$ (34b)

Now our aim is to solve Eqs. (31a)-(34b). We multiply Eqs. (31a), (31b) by $\psi_{n,2}(y)$ and then integrating it over (d,h_0) for obtaining the unknowns. Hence, we get:

$$\int_d^{h_0}\phi_1(-l,y)\psi_{n,2}(y)\mathrm{d}y=\int_d^{h_0}\phi_2(-l,y)\psi_{n,2}(y)\mathrm{d}y,$$

$n=0,1,2,\cdots,N$ (35a)

$$\int_0^{h_0}\phi_{1x}(-l,y)\psi_{n,2}(y)\mathrm{d}y=\int_d^{h_0}\phi_{2x}(-l,y)\psi_{n,2}(y)\mathrm{d}y,$$

$n=0,1,2,\cdots,N$ (35b)

$\phi_{1x}=0$ at $x=-l$, $0\le y\le d$ is used in Eq. (35b).

Multiplying by $\psi_{n,j}(y)$ and $\psi_{n,j+1}(y)$, $j=2,3,\cdots,m+2$ in both sides of Eqs. (32a), (32b) respectively and integrating over $(0,h_{j-2})$, we get

$$\int_d^{h_{j-2}}\phi_j(-a_{m+2-j},y)\psi_{n,j}(y)\mathrm{d}y=$$

$$\int_d^{h_{j-2}}\phi_{j+1}(-a_{m+2-j},y)\psi_{n,j}(y)\mathrm{d}y,$$

$n=0,1,2,\cdots,N$ (36a)

$$\int_d^{h_{j-2}}\phi_{jx}(-a_{m+2-j},y)\psi_{n,j+1}(y)\mathrm{d}y=$$

$$\int_d^{h_{j-1}}\phi_{(j+1)x}(-a_{m+2-j},y)\psi_{n,j+1}(y)\mathrm{d}y,$$

$n=0,1,2,\cdots,N$ (36b)

using the condition $\phi_{(j+1)x}(-a_{m+2-j},y)=0$, $h_{j-2}<y<h_{j-1}$, $j=2,3,\cdots,m+2$ in the Eq. (36b).

We multiply by $\psi_{n,j+1}(y)$ and $\psi_{n,j}(y)$, $j=m+3,m+4,\cdots,2m+2$ in both sides of Eqs. (33a), (33b) respectively and integrating it over $(0,h_{j-1})$

$$\int_d^{h_{j-1}}\phi_j(a_{j-(m+2)},y)\psi_{n,j+1}(y)\mathrm{d}y=$$

$$\int_{d}^{h_{j-1}} \phi_{j+1}(a_{j-(m+2)}, y)\psi_{n,j+1}(y)\mathrm{d}y\,,$$

$$n = 0,1,2,\cdots,N \tag{37a}$$

$$\int_{d}^{h_{j-2}} \phi_{jx}(a_{j-(m+2)}, y)\psi_{n,j}(y)\mathrm{d}y =$$

$$\int_{d}^{h_{j-1}} \phi_{(j+1)x}(a_{j-(m+2)}, y)\psi_{n,j}(y)\mathrm{d}y\,,$$

$$n = 0,1,2,\cdots,N \tag{37b}$$

using the condition $\phi_{jx}(a_{j-(m+2)}, y) = 0$, $h_{j-1} < y < h_{j-2}$, $j = m+3, m+4, \cdots, 2m+2$ in the Eq. (37b).

Further, we multiply Eqs. (34a), (34b) by $\psi_{n,2m+3}(y)$ and integrating it over $(d, \hat{h}_0)$

$$\int_{d}^{\hat{h}_0} \phi_{2m+3}(l,y)\psi_{n,2m+3}(y)\mathrm{d}y = \int_{d}^{\hat{h}_0} \phi_{2m+4}(l,y)\psi_{n,2m+3}(y)\mathrm{d}y\,,$$

$$n = 0,1,2,\cdots,N \tag{38a}$$

$$\int_{d}^{\hat{h}_0} \phi_{(2m+3)x}(l,y)\psi_{n,2m+3}(y)\mathrm{d}y =$$

$$\int_{0}^{\hat{h}_0} \phi_{(2m+4)x}(l,y)\psi_{n,2m+3}(y)\mathrm{d}y\,,$$

$$n = 0,1,2,\cdots,N \tag{38b}$$

$\phi_{(2m+4)x} = 0$ at $x = l$, $0 \le y \le d$ is used in Eq. (38b). Truncating each of the series in Eqs. (15)-(20) up to N (say), the Eqs. (35a)-(38b) produce a system of linear algebraic equations of size $(4m+6)N + (4m+6)$ which need to be solved to get the unknowns R, T, A_n, $B_{0,j}$, $C_{0,j}$, $B_{n,j}$, $C_{n,j}$, D_n, where $j = 2,3,\cdots,2m+3$ and $n = 1,2,\cdots,N$.

1.3 *In the presence of wall*

In this section, the problem of wave-structure interaction over arbitrary bottom topography is considered when a vertical rigid wall is situated at $x = L$ as shown in Fig. 2. The regions from R_1 to R_{2m+3} are same as defined in Section 1.1 "In absence of wall" and the last region R_{2m+4} is $l \le x \le L$, $0 \le y \le \hat{h}_0$ Here, the associated mixed boundary value problem (BVP) will remain same as discussed in section "In absence of wall". In addition to this, we will have a condition on the wall. Due to the rigidity of the vertical wall, the boundary condition at $x = L$ will be

$$\frac{\partial \phi_{2m+4}}{\partial x} = 0\,,\quad x = L,\quad 0 \le y \le \hat{h}_0 \tag{39}$$

Now, we will follow the eigenfunction expansion procedure as discussed in Section 1.2 to solve the bvp involving Eqs. (1)-(14) and (39). Once ϕ_j, $j = 1,2,\cdots,2m+4$ are obtained, the force on the wall in the presence of rigid dock, towards the reduction of high wave load on the wall, can be calculated which is the main concern here. The expressions for velocity potentials ϕ_j, $j = 1,2,\cdots,2m+3$ remain the same as defined in Eqs. (15)-(30), but the velocity potential ϕ_{2m+4} becomes

$$\phi_{2m+4}(x,y) = \hat{D}_0 \cos p_{0x}(x-L)g_0(y) + \sum_{n=1}^{\infty} \hat{D}_n \cosh p_{nx}(x-L)g_n(y) \tag{40}$$

where $\hat{D}_n$, $n = 0,1,2,\cdots$ along with other unknowns R, A_n, $B_{0,j}$ $C_{0,j}$, $B_{n,j}$, $C_{n,j}$, $j = 2,3,\cdots,2m+3$ and $n = 1,2,\cdots$ are to be determined. The Eqs. (31a)-(34b) towards the continuity of pressure and velocity at all interfaces give rise the Eqs. (35a)-(38b) which need to be solved to obtained the unknowns.

1.4 *Force exercised by the floating dock and wall*

The force components involving horizontal force F_x and vertical force F_y exercised by the floating dock (with and without wall) for unit amplitude incident wave are of the forms:

$$F_x = \mathrm{i}\omega\rho \mathrm{e}^{-\mathrm{i}k_0 l} \times \int_{d}^{0} [\phi_1(-l,y) - \phi_{2m+4}(l,y)]\mathrm{d}y \tag{41}$$

and

$$F_y = \mathrm{i}\omega\rho \mathrm{e}^{-\mathrm{i}k_0 l} \times \int_{-l}^{l} \phi\big|_{y=d}\,\mathrm{d}x \tag{42}$$

The force namely the horizontal force F_{wall} experienced by the wall is derived as

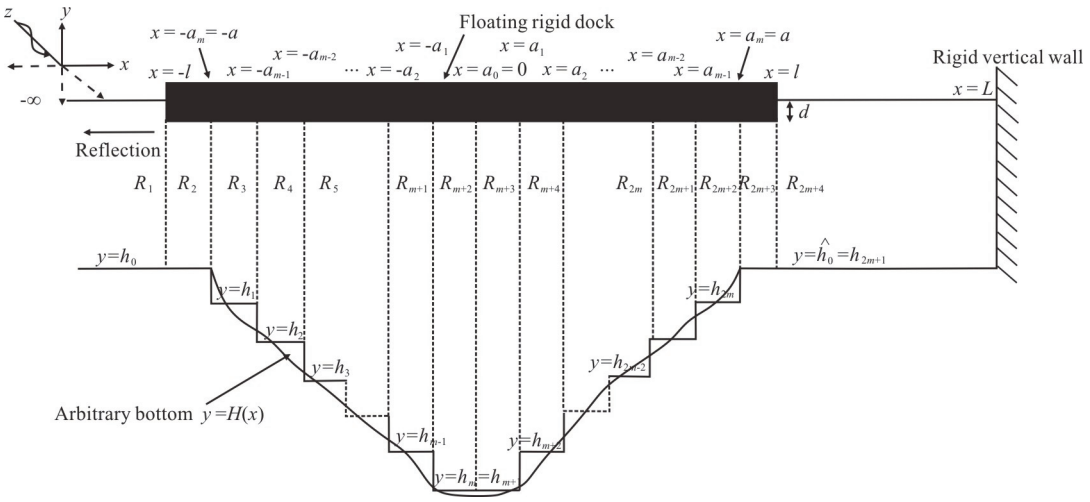

Fig. 2 Physical problem in the presence of wall

$$F_{\text{wall}} = \mathrm{i}\omega\rho \mathrm{e}^{-\mathrm{i}k_0 l} \times \int_{\hat{h}_0}^{0} \phi_{2m+4}(L,y)\mathrm{d}y \tag{43}$$

The surface elevations denoted by η_1 and η_{2m+4} respectively, in region R_1 and R_{2m+4} can be obtained as

$$\eta_j = \mathrm{i}\omega \left.\frac{\partial \phi_j}{\partial y}\right|_{y=0}, \quad j = 1, 2m+4 \tag{44}$$

2. Results and discussion

2.1 *In the absence of wall*

In this section, the hydrodynamic quantities namely, T, R, F_x, F_y and $Re(\eta_{2m+4})$ are determined. Here, all the structural and system parameters are non-dimensionalized by using length scale h_0. The non-dimensional parameters are given by $\hat{l} = l/h_0$, $\hat{d} = d/h_0$, $\hat{a}_i = a_i/h_0$, $i = 1,2,\cdots,m$, $K_1 = Kh_0$, $H_j = h_j/h_0$, $j = 1,2,\cdots,2m+1$ and $\hat{F}_x = F_x/\rho g l$, $\hat{F}_y = F_y/\rho g l$ which are used for numerical computations. The values of $\hat{a}_i$, $i = 1,2,\cdots,m-1$ for flat and rectangular bottoms, triangular and parabolic type bottoms, are obtained using the formula $\hat{a}_i = i(\hat{a}_m/m)$, $i = 1,2,\cdots,m-1$ by fixing the value of $\hat{a}_m$. The values of $\hat{a}_i$, $i = 2,3,\cdots,m-1$ for trapezoidal bottom are obtained using the formula $\hat{a}_i = \hat{a}_i + (i-1)[(\hat{a}_m - \hat{a}_i)/(m-1)]$, $i = 2,3,\cdots,m-1$ by fixing the values of $\hat{a}_1$ and $\hat{a}_m$. The values of $\hat{a}_m = 0.5$, $\hat{l} = 1.0$, $\hat{d} = 0.4$, $H_0 = 1.0$, $H_{2m+1} = 1.2$ and $H_m = H_{m+1} = 2.0$ (since $H_m \geq H_{2m+1}$ in the given problem) and $\theta = \pi/4$ are fixed in the study unless otherwise stated. The other depth ratios $H_j\,(j = 1,2,\cdots,m-1,m+2,m+3,\cdots,2m)$ are calculated using different formula depending upon the type of irregular topography. Several computational results are performed to analyse the effect of various system parameters but in the subsequent section, few results are shown to avoid the similar behaviour of figures.

2.1.1 Validation: Comparison with results of "rigid dock over flat bottom"

To validate the present results with Linton[1] for a rigid dock over flat bottom (Reference Fig. 3), the depth ratios $H_j = 1$, $j = 0,1,\cdots,2m+1$, $\hat{d} = 0$, $\hat{l} = 1.0$ and $\theta = \pi/4$ are considered in the said problem. The results are well matched (Fig. 4) with the results by Linton[1] who used the modified residue calculus technique for this particular case.

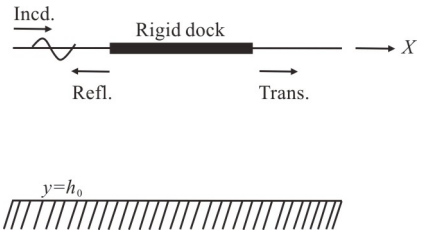

Fig. 3 Finite rigid dock over flat bottom

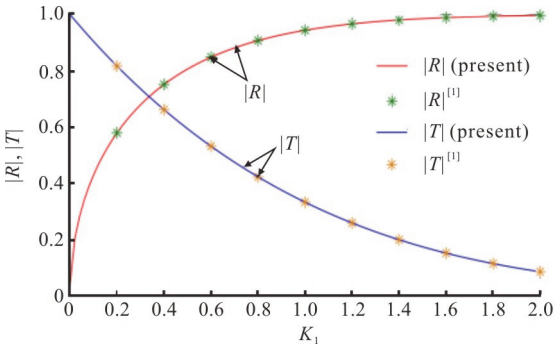

Fig. 4 (Color online) $|R|$ and $|T|$ versus K_1 for fixed $H_j = 1$, $j = 0,1,\cdots,2m+1$

2.1.2 Convergence study on m and N

In this section, the convergence on m (number of successive steps either in downward direction or in upward direction) and N (number of evanescent modes) is examined for symmetric parabolic type bottom profile (Fig. 6(a)). We know that $2m$ numbers of successive steps are required to approximate the profile. For convergence of N we fix $m = 240$ and the values of $|R|$ and $|T|$ are depicted against K_1 for various values of $N = 1$, 5, 10 and 15 (see Fig. 5). This figure shows that the curve of $|R|$ (also $|T|$) for $N = 10$ is coinciding with the curve for $N = 15$. Hence, $N = 10$ is considered throughout the study.

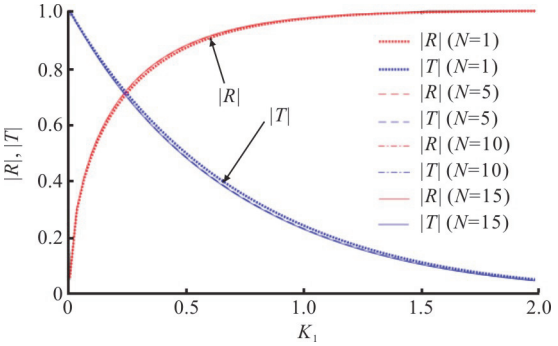

Fig. 5 (Color online) $|R|$ and $|T|$ versus K_1 for fixed value of $m = 240$ and different values of N

For convergence of m the number of evanescent modes N is fixed as 10 and $|R|$ and $|T|$ are calculated for different values of $m = 60$, 180, 240, 280 and 300 (see Table 1). Table 1 shows that same values of $|R|$ and $|T|$ are obtained up to four decimal places for $m = 240$, 280 and 300 and fixed values of K_1. Further, for all numerical calculations

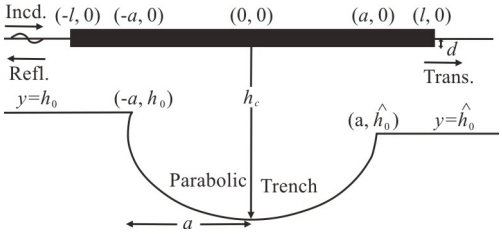

Fig. 6(a) Finite rigid dock over asymmetric parabolic bottom

Table 1 Numerical values of $|R|$ and $|T|$ versus K_1 for $N = 10$ and different values of m

K_1	m	$\lvert R\rvert$	$\lvert T\rvert$	$\lvert R\rvert^2 + \gamma\lvert T\rvert^2$
0.3	60	0.768924	0.639300	0.999950
	180	0.768282	0.640072	0.999950
	240	0.768149	0.640231	0.999950
	280	0.768088	0.640305	0.999950
	300	0.768062	0.640335	0.999950
0.5	60	0.878999	0.476725	0.999907
	180	0.878556	0.477540	0.999907
	240	0.878465	0.477709	0.999907
	280	0.878422	0.477787	0.999907
	300	0.878404	0.477820	0.999907
1.0	60	0.974224	0.225287	0.999868
	180	0.974103	0.225810	0.999867
	240	0.974077	0.225920	0.999867
	280	0.974065	0.225971	0.999867
	300	0.974060	0.225993	0.999867

related to parabolic bottom, $m = 240$ i.e., 480 steps and $N = 10$ are considered throughout this study unless otherwise stated.

2.1.3 Energy conservation principle

The numerical values of $|R|$ and $|T|$ obtained by the present method are found to validate the energy conservation principle, as given by the following relation

$$|R|^2 + \gamma |T|^2 = 1 \tag{45}$$

where

$$\gamma = \left(\frac{k_0 p_{0x}}{p_0 k_{0x}}\right)\frac{2p_0\hat{h}_0 + \sinh 2p_0\hat{h}_0}{2k_0h_0 + \sinh 2k_0h_0}\left(\frac{\cosh^2 k_0h_0}{\cosh^2 p_0\hat{h}_0}\right)$$

In Table 1, $|R|$ and $|T|$ are tabulated for different values of K_1 and $\theta = \pi/4$ The last column of the Table 1 reflects that the energy conservation identity (45) is verified.

2.1.4 Reflection and transmission by a rigid dock over different bottom

In this section, we consider four kinds of asymmetric bottom topography namely parabolic type (Fig. 6(a)), trapezoidal trench (Fig. 6(b)), rectangular trench (Fig. 7(a)), triangular trench (Fig. 7(b)). The equations for parabolic trench, trapezoidal trench and triangular trench are given by Eqs. (46)-(48) respectively:

$$H(x)=h_0,\quad x<-a \tag{46a}$$

$$H(x)=h(x)=h_c\left(1-\frac{x^2}{\alpha^2}\right),\quad -a\le x\le a \tag{46b}$$

$$H(x)=\hat{h}_0,\quad a\le x \tag{46c}$$

where $\alpha=a/\sqrt{1-h_0/h_c}$ (see Jung et al.[21] for details).

$$H(x)=h_0,\quad x\le -a \tag{47a}$$

$$H(x)=h_0+\left(\frac{h_c-h_0}{a-a_1}\right)(x+a),\quad -a\le x\le -a_1 \tag{47b}$$

$$H(x)=h_c,\quad -a_1\le x\le a_1 \tag{47c}$$

$$H(x)=\hat{h}_0+\left(\frac{h_c-\hat{h}_0}{a_1-a}\right)(x-a),\quad a_1\le x\le a \tag{47d}$$

$$H(x)=\hat{h}_0,\quad a\le x \tag{47e}$$

$$H(x)=h_0,\quad x\le -a \tag{48a}$$

$$H(x)=h_0+\left(\frac{h_c-h_0}{a}\right)(x+a),\quad -a\le x\le 0 \tag{48b}$$

$$H(x)=\hat{h}_0+\left(\frac{h_c-\hat{h}_0}{a}\right)(a-x),\quad 0\le x\le a \tag{48c}$$

$$H(x)=\hat{h}_0,\quad a\le x \tag{48d}$$

where h_c denotes the water depth at the centre of the bottom profile and a the half-width of the profile and $h_0=\hat{h}_0$ gives rise the symmetric bottom profile. After approximating the profile using steps, we get $h_c=h_m$, $\hat{h}_0=h_{2m+1}$.

(1) Effect due to absence and presence of dock over rectangular bottom

The curves of $|R|$ and $|T|$ are depicted against K_1 in Fig. 8(a) in the presence and absence of dock for rectangular (Fig. 7(a)) bottom profile with $H_m=2.5$, $H_{2m+1}=0.5$, $\hat{a}_1=2.5$, $\theta=0°$ $\hat{l}=3.0$ To differentiate between the results of absence and presence of dock over rectangular bottom, we have compared the present results with Roy et al.[22]. It is noticed from the graph that less energy is transmitted to sea side in presence of dock. Same observation can be obtained for other cases of bottom profile.

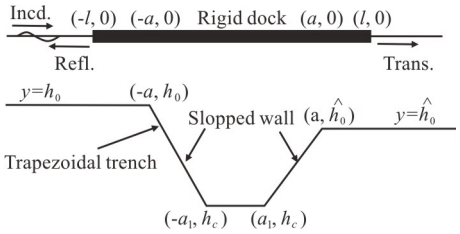

Fig. 6(b) Finite rigid dock over asymmetric trapezoidal bottom

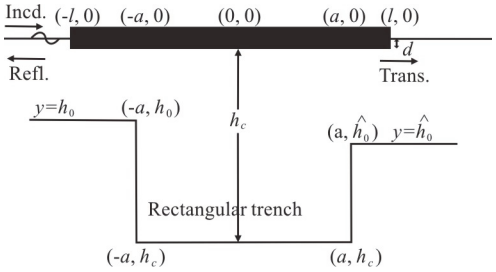

Fig. 7(a) Finite rigid dock over asymmetric rectangular bottom

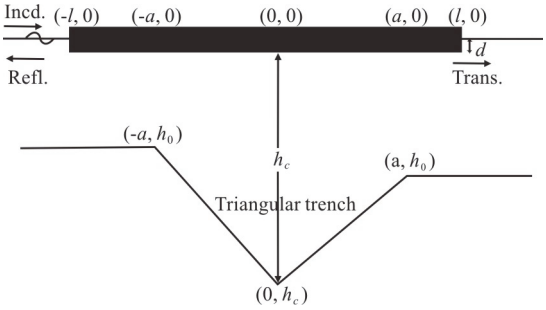

Fig. 7(b) Finite rigid dock over asymmetric triangular bottom

(2) Effect of parabolic bottom profile

We have plotted $|R|$ and $|T|$ against K_1 in Fig. 8(b) for $\theta=\pi/3$ to observe the effect of arbitrary bottom (in particular, symmetric parabolic bottom here) as compared to flat bottom ($H_j=1$, $j=0,1,\cdots,2m+1$) in presence of dock. It is observed that more energy is reflected back due to the presence of parabolic bottom, resulting less energy is transmitted

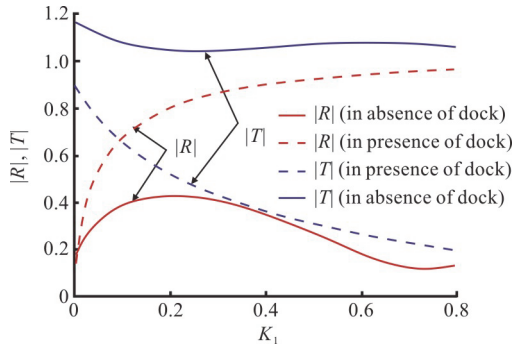

Fig. 8(a) (Color online) $|R|$ and $|T|$ in absence and presence of dock over rectangular bottom

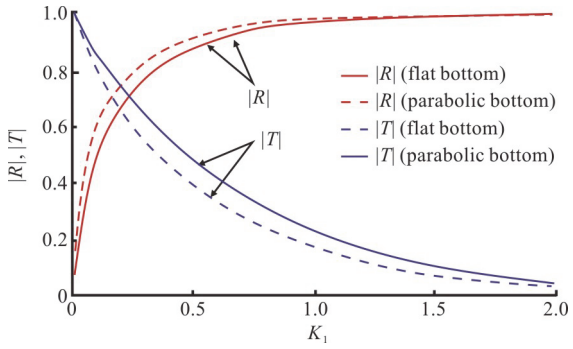

Fig. 8(b) (Color online) $|R|$ and $|T|$ in presence of dock over flat and parabolic bottom

towards sea side. As a consequence, sea shore is protected, which accomplish the aim of this study. Now onwards, parabolic bottom is taken to obtain the other numerical results in the subsequent sections.

2.1.5 Effect of system parameters on reflection and transmission

In this section, we consider an asymmetric parabolic bottom profile given by Eq. (46). The results of various structural variables such as length of dock, dock thickness, water depth ratios and angle of incidence on hydrodynamic quantities are analyzed and discussed.

(1) Effect of the dock length and thickness, water depth ratios

The graphical representations of $|R|$ and $|T|$ versus K_1 for various values of $\hat{l}$ = 1.0, 1.5 and 2.0 are depicted in Fig. 9(a). It is viewed that for shorter waves i.e., larger values K_1, $|R|$ becomes almost one which happens due the fact that shorter waves confined near the free surface and almost reflected back by the floating structure. It is also viewed that larger values of dock length produces more reflection, resulting less transmission. Further, it is viewed from the computational results that similar behaviour of $|R|$ and $|T|$ as function of dock thickness and as a function of water depth ratios can be obtained.

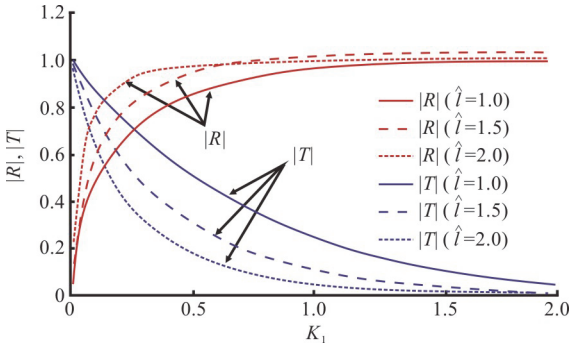

Fig. 9(a) (Color online) The effect of dock length on $|R|$ and $|T|$

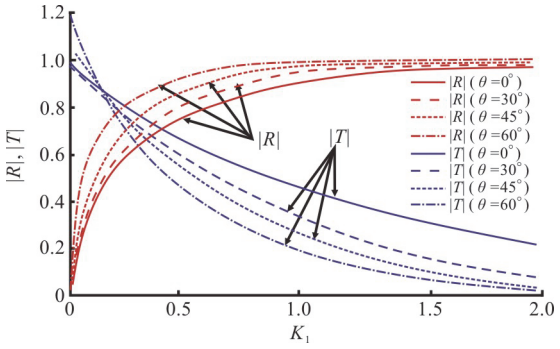

Fig. 9(b) (Color online) The effect of angle of incidence on $|R|$ and $|T|$

(2) Effect of angle of incidence

The effect of angle of incidence (θ) on $|R|$ and $|T|$ shown in Fig. 9(b). Here the values of θ=0°, 30°, 45° and 60° are considered. It is observed that for normal incidence $\theta = 0°$ less reflection is observed as compared to other angles of incidence. Moreover, more energy is reflected back as the angle of incidence is increased, consequently less energy will be transmitted to sea-side.

(3) Force experienced by dock

Horizontal force $(|\hat{F}_x|)$ and vertical force $(|\hat{F}_y|)$ components acting on dock in presence of asymmetric parabolic bottom profile is calculated and analyzed for various system parameters. Figures 10(a) and 10(b) show the variation of $(|\hat{F}_x|)$ and $(|\hat{F}_y|)$ acting on the floating dock with respect to K_1 for various values of $\hat{l}$ = 1.0, 1.5 and 2.0. It is observed that $(|\hat{F}_x|)$

increases, ($|\hat{F}_y|$) decreases for larger values of K_1 which happens due to the fact that shorter waves confined near the free surface and almost reflected back by floating structure. Further, it is noticed that increment in the length of the dock yields less vertical force ($|\hat{F}_y|$) and horizontal force ($|\hat{F}_x|$) as shown in Figs. 10(a) and 10(b). This is due to the fact that larger value of dock length, more wave energy will be reflected back; hence less horizontal as well as vertical force will be experienced by the dock.

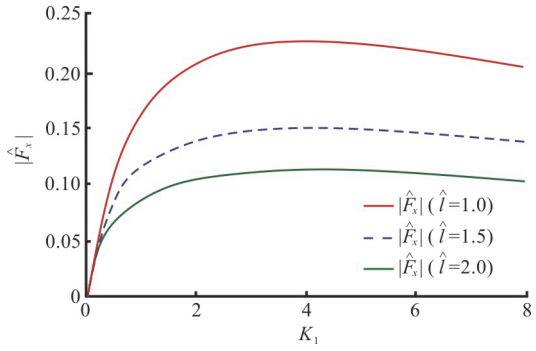

Fig. 10(a) (Color online) Effect of dock length on horizontal force ($|\hat{F}_x|$) against K_1

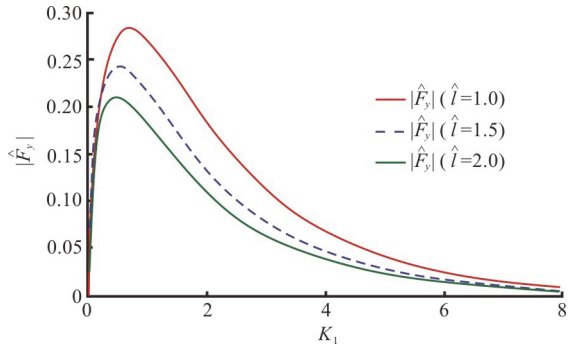

Fig. 10(b) (Color online) Effect of dock length on vertical force ($|\hat{F}_y|$) against K_1

The effect of angle of incidence θ on horizontal and vertical forces for various values of dock length is shown in Figs. 11(a) and 11(b). It is found that less vertical as well as horizontal forces are experienced by dock for larger values of θ. Further, almost zero vertical and horizontal forces are experienced by the dock for $\theta > 88°$. Moreover, same effect of dock length on forces is obtained against θ as mentioned in Figs. 10 (a) and 10(b).

In Figs. 12(a) and 12(b), ($|\hat{F}_x|$) and ($|\hat{F}_y|$) are depicted against K_1 for various values of $\hat{d}$. It is noted that an increment in dock thickness yields less

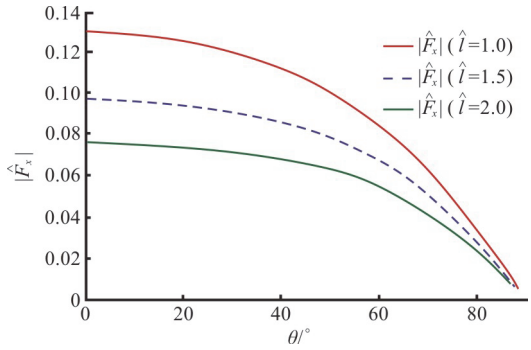

Fig. 11(a) (Color online) Effect of dock length on horizontal force ($|\hat{F}_x|$) against θ

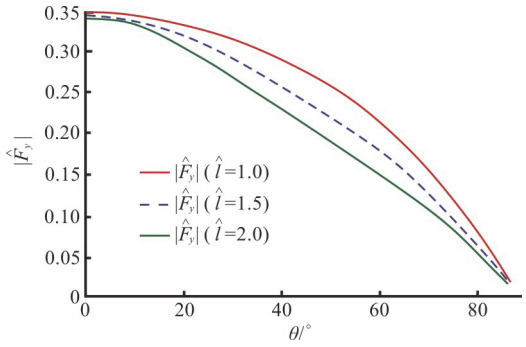

Fig. 11(b) (Color online) Effect of dock length on vertical force ($|\hat{F}_y|$) against θ

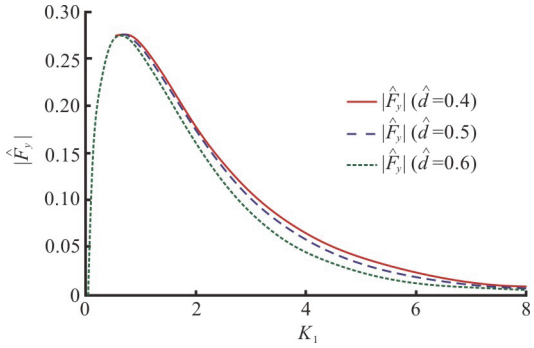

Fig. 12(a) (Color online) Effect of dock thickness on vertical force ($|\hat{F}_y|$)

vertical force ($|\hat{F}_y|$) (Fig. 12(a)) and more horizontal force ($|\hat{F}_x|$) (Fig. 12(b)). This is plausible because wider the thickness, producing more reflection causing more horizontal force and less vertical force.

The effect of angle of incidence θ on force components ($|\hat{F}_x|$) and ($|\hat{F}_y|$) is depicted in Figs. 13(a) and 13(b). Here the values of $\theta = 10°, 25°, 50°$

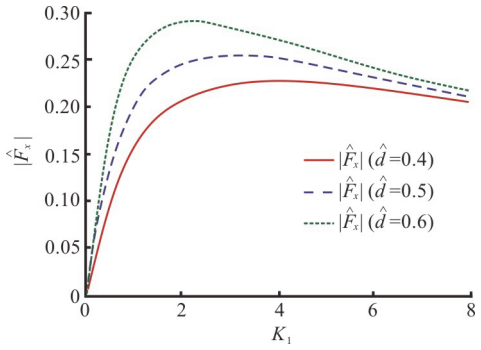

Fig. 12(b) (Color online) Effect of dock thickness on horizontal force ($|\hat{F}_x|$)

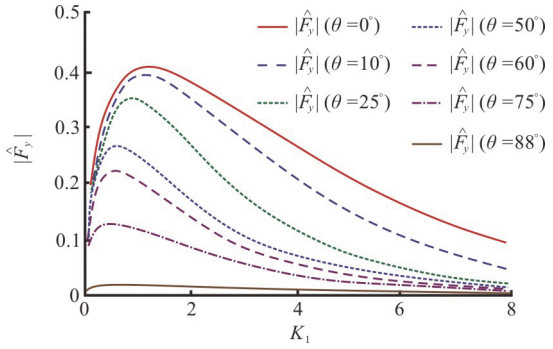

Fig. 13(a) (Color online) Effect of angle of incidence on vertical force ($|\hat{F}_y|$)

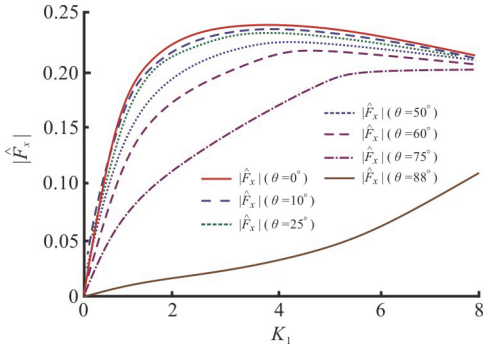

Fig. 13(b) (Color online) Effect of angle of incidence on horizontal force ($|\hat{F}_x|$)

and 60°, 75°, 88° are considered to examine the effect. It is observed that the global maximum of the force component is very small for $\theta = 88°$ as compared to other angles of incidence. This happens due to the fact that for $\theta = 88°$ the incident waves are almost perpendicular to the dock.

(4) Wave elevation profile in last region R_{2m+4}

Figures 14(a) shows the behaviour of wave elevation $Re(\eta_{2m+4})$ in the region R_{2m+4} for different values of $\hat{l}$ = 1.0, 1.5 and 2.0. It is noticed that wave amplitude decreases as the length of the dock increases. It is viewed from the computational results that similar behaviour of wave elevation $Re(\eta_{2m+4})$ as a function of dock thickness and as a function of water depth ratios can be obtained. The effect of angle of incidence $\theta = 30°$, 45°, 60° is shown in Fig. 14(b). It is noticed from Fig. 14(b) that the wave amplitude decreases whereas wavelength increases as θ increases as observed by Bhattacharjee and Soares[18]. Consequently, less energy is transmitted to sea side in all the cases, resulting sea shore is protected. In both the cases, this phenomenon is in accord with the physical behaviour of the said problem.

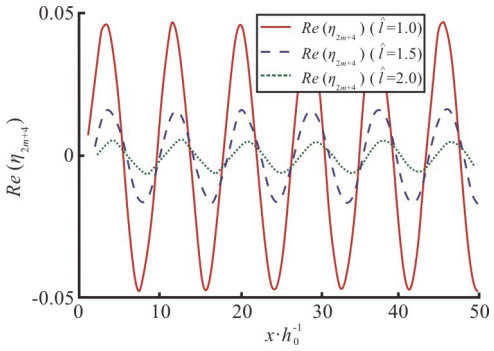

Fig. 14(a) (Color online) Effect of dock length $\hat{l}$ on wave elevation $Re(\eta_{2m+4})$ in last region for fixed K_1 = 0.5

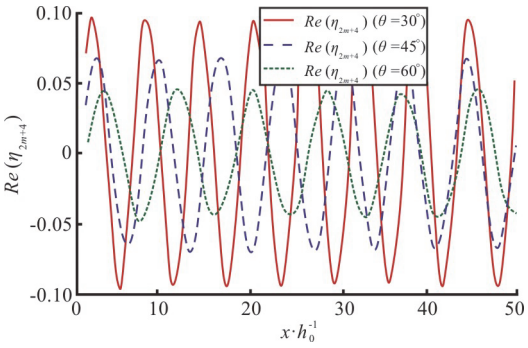

Fig. 14(b) (Color online) Effect of angle of incidence θ on wave elevation $Re(\eta_{2m+4})$ in last region for fixed $K_1 = 0.5$

2.2 *In the presence of wall*

In the subsequent section, the numerical results for $Re(\eta_{2m+4})$ and $|\hat{F}_{\text{wall}}| = |F_{\text{wall}}|/\rho g l$ for asymmetric parabolic bottom profile are graphically depicted to examine the effect of various system parameters. In addition to the system parameters considered in Section 2.1, the gap denoted by $\hat{L} = L/h_0 = 4.0$ is

fixed throughout this section unless otherwise stated.

Here our aim is to analysis how much force will be experienced by the seawall for different values of system parameters so that the seawall can be protected. It is natural that there will be full reflection and no transmission due to the presence of seawall.

(1) Effect of dock and parabolic bottom topography on seawall

Force experienced by seawall $(|\hat{F}_{\text{wall}}|)$ for flat bottom $(H_j = 1.0, j = 0,1,..,2m+1)$ and parabolic bottom are depicted graphically against K_1 in Fig. 15 for fixed value of $\theta = \pi/4$ The figure reveals that less force is experienced by the seawall in presence of parabolic bottom. Hence, arbitrary bottom profile (parabolic profile here) provides the structural safety and stability of the seawall.

(2) Effect of system parameters on force acting on seawall

The effect of dock length $\hat{l}$ on $(|\hat{F}_{\text{wall}}|)$ is illustrated in Fig. 16(a). Here, the force $(|\hat{F}_{\text{wall}}|)$ is depicted against θ for fixed value of $K_1 = 1.0$. It is noted that as the length of dock increases, the force experienced by the wall decreases. This is due to the fact that more incident wave energy is reflected back as the length of the dock increases, hence less force is experienced by the rigid wall. Further, it is found that the wall experiences almost zero force for $\theta > 70°$. It is viewed from the computational results that similar behaviour for the force as a function of dock thickness can be obtained. Further, the sharp peaks in figure are due to the mutual interaction between the reflected wave and incident wave in region R_{2m+4}. The Fig. 16(b) shows the effect of gap on $(|\hat{F}_{\text{wall}}|)$ where the gap between the rigid wall and floating dock is being taken from the center of dock. It is observed from figure that less load on the seawall is found for lower value of θ when the gap increases.

(3) Effect of system parameters on wave elevations

In Fig. 17 wave elevation $Re(\eta_1)$ (in the region R_1) depicted graphically for fixed values of $K_1 = 1.0$, $\hat{l} = 1.0$, $\hat{d} = 0.4$ and $\hat{L} = 50$. The Fig. 18(a) shows the effect of dock length $\hat{l}$ on wave elevation $Re(\eta_{2m+4})$ in last region. From Fig. 18 (a) it is clear that wave amplitude in region R_{2m+4} decreases as the length of dock increases. The Fig. 18(b) shows the effect of gap $\hat{L}$ on wave elevation in last region. From this figure, it is clear that wave amplitude decreases as the gap increases. Figures 18(a) and 18(b) show that the wave amplitude in the last region R_{2m+4} is very small as compared to wave amplitude in the first region (see Fig. 17), which indicates that the calm zone between floating dock and rigid seawall is created. Hence, seawall is protected.

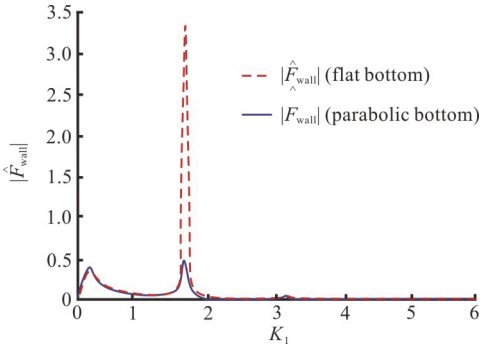

Fig. 15 (Color online) Horizontal force $(|\hat{F}_{\text{wall}}|)$ over flat and parabolic bottom in presence of dock

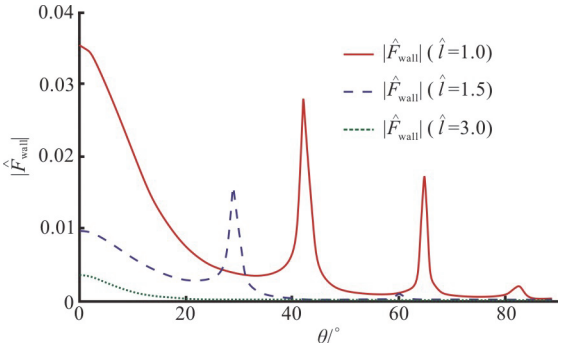

Fig. 16(a) (Color online) Effect of dock length on $(|\hat{F}_{\text{wall}}|)$

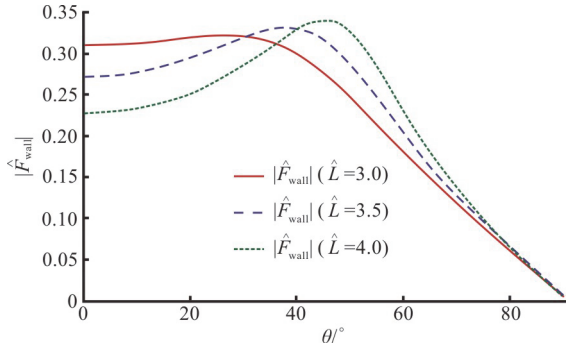

Fig. 16(b) (Color online) Effect of gap between seawall and dock on $(|\hat{F}_{\text{wall}}|)$

3. Conclusions

The three-dimensional problem involving diffrac-

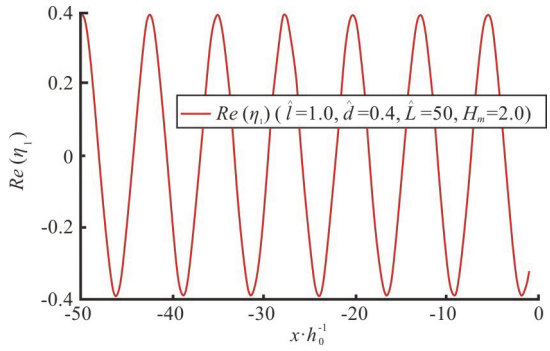

Fig. 17 (Color online) Wave elevation $Re(\eta_1)$ in presence of wall for fixed $K_1 = 1.0$

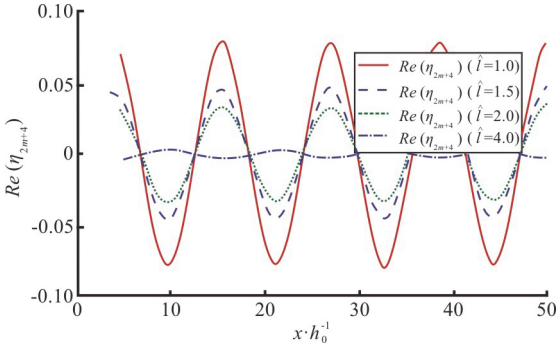

Fig. 18(a) (Color online) Effect of dock length on wave elevation $Re(\eta_{2m+4})$ for fixed $K_1 = 1.0$

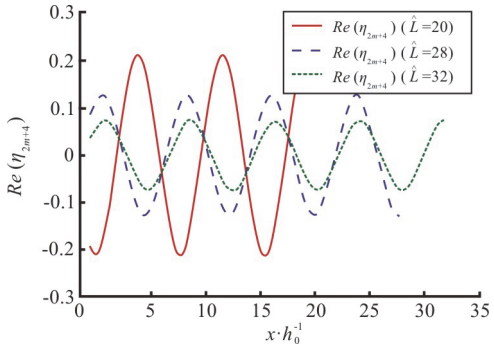

Fig. 18(b) (Color online) Effect of gap on wave elevation $Re(\eta_{2m+4})$ for fixed $K_1 = 1.0$

tion of water waves by a finite floating thick rigid dock over an arbitrary bed is studied for two cases (1) in the absence of wall, (2) in the presence of wall. The uneven shape is approximated by a series of steps for which m number of steps are taken in downward direction and m number of steps is taken in upward direction. The step approximation followed by matched eigenfunction expansion method yields a system of equations, which is solved to determine the numerical values of hydrodynamic quantities. The effect of various structural parameters, such as length, thickness of dock and gap between dock and seawall, water depth and angle of incidence on the reflection, transmission and force is examined through different graphs. In the absence of wall the present results have been validated by the known results[1]. The energy identity is checked which verifies the accuracy of numerical results.

In the absence of wall: (1) $|T|$ decreases and $|R|$ increases when the dock is situated over parabolic bottom profile instead of flat bottom for oblique wave incidence. (2) $|T|$ decreases and $|R|$ increases when dock thickness $\hat{d}$, dock length $\hat{l}$, water depth ratios and angle of incidence θ increases. (3) The horizontal force increases for larger values of K_1 whereas vertical force decreases. (4) The vertical force acting on the floating dock decreases as the dock length (also dock thickness) increases. (5) The horizontal force acting on the floating dock decreases as the dock length increases but horizontal force increases for larger values of dock thickness. (6) Both the force components decrease as angle of incidence increases and almost zero force experienced by dock for $\theta > 88°$ (7) The wave amplitude in the last region (free region) decreases as the length; thickness of the dock; angle of incidence and water depth increases. These facts help to coastal and marine scientist to construct the offshore structures to protect the beach-side.

In the presence of wall: (1) Less horizontal force on seawall is experienced when the dock is situated over the parabolic bottom instead of flat bottom for oblique wave incidence. (2) Since more incidents wave energy is reflected back by longer the length as well as the thickness of the dock, hence, less force is experienced by seawall. (3) By placing a floating structure at a finite distance from the seawall, the high wave load on the seawall can be reduced. (4) If the gap between the seawall and dock is least then more force is experienced by the seawall for smaller values of θ whereas reverse behavior of force is observed for larger value of θ. Hence, the length and thickness of the dock, gap between the dock and seawall, angle of incidence and water depth can be modified to optimize the wave load on the rigid seawall. (5) It is observed that wave amplitude in the last region decreases as the length of the dock, the thickness of the dock, gap between the seawall and dock, water depth increases. Moreover, the wave amplitude in the last region (after the dock) is very small as compared to amplitude in the first region (before the dock). This provides a tranquillity zone between the floating dock and the rigid seawall, which is useful for the harbour areas (for example, the calm zone will provide a safe mooring-loading operations and comfortable handling

of cargoes and ships). This study will provide an immense support to coastal engineers for the construction of offshore structures so that seashore as well as seawall can be protected.

Acknowledgment

The authors thank the reviewers and associate editor of Journal of Hydrodynamics for their comments and suggestions to improve the article in the present form. A. Kaur thanks DST, India for support through inspire fellowship.

References

[1] Linton C. M. The finite dock problem [J]. *Zeitschrift Fr Angewandte Mathematik und Physik ZAMP*, 2001, 52(4): 640-656.

[2] Chakrabarti A., Mandal B. N., Gayen R. The dock problem revisited [J]. *International Journal of Mathematics and Mathematical Sciences*, 2005, 21: 3459-3470.

[3] Cho I. H., Kim M. H. Interactions of a horizontal flexible membrane with oblique incident waves [J]. *Journal of Fluid Mechanics*, 1998, 367: 139-161.

[4] Martha S. C., Bora S. N. Reflection and transmission coefficients for water wave scattering by a sea-bed with small undulation [J]. *Journal of Applied Mathematics and Mechanics*, 2007, 87(4): 314-321.

[5] Xie J., Liu H. W. An exact analytic solution to the modified mild-slope equation for waves propagating over a trench with various shapes [J]. *Ocean Engineering*, 2012, 50: 72-82.

[6] Lin P., Liu H. W. Analytical study of linear-wave reflection by a two-dimensional obstacle of general trapezoidal shape [J]. *Journal of Engineering Mechanics*, 2005, 131(8): 822-830.

[7] Xie J. J., Liu H. W., Lin P. Analytical solution for long-wave reflection by a rectangular obstacle with two scour trenches [J]. *Journal of Engineering Mechanics*, 2011, 137(12): 919-930.

[8] Wang C. D., Meylan M. H. The linear wave response of a floating thin plate on water of variable depth [J]. *Applied Ocean Research*, 2002, 24(3): 163-174.

[9] Xu F., Lu D. Q. An optimization of eigenfunction expansion method for the interaction of water waves with an elastic plate [J]. *Journal of Hydrodynamics*, 2009, 21(4): 526-530.

[10] Karmakar D., Sahoo T. Gravity wave interaction with floating membrane due to abrupt change in water depth [J]. *Ocean Engineering*, 2008, 35(7): 598-615.

[11] Dhillon H., Banerjea S., Mandal B. N. Water wave scattering by a finite dock over a step-type bottom topography [J]. *Ocean Engineering*, 2016, 113: 1-10.

[12] Guo Y. X., Liu Y., Meng X. Oblique wave scattering by a semi-infinite elastic plate with finite draft floating on a step topography [J]. *Acta Oceanologica Sinica*, 2016, 35(7): 113-121.

[13] Das S., Bora S. N. Reflection of oblique ocean water waves by a vertical porous structure placed on a multi-step impermeable bottom [J]. *Applied Ocean Research*, 2014, 47: 373-385.

[14] Meng Q. R., Lu D. Q. Scattering of gravity waves by a porous rectangular barrier on a seabed [J]. *Journal of Hydrodynamics*, 2016, 28(3): 519-522.

[15] Zhao W., Taylor P. H., Wolgamot H. A. et al. Amplification of random wave run-up on the front face of a box driven by tertiary wave interaction [J]. *Journal of Fluid Mechanics*, 2019, 869: 706-725.

[16] Liu Y., Li Y. C., Teng B. Wave interaction with a new type perforated breakwater [J]. *Acta Mechanica Sinica*, 2007, 23(4): 351-358.

[17] Liu Y., Li Y., Teng B. Interaction between obliquely incident waves and an infinite array of multi-chamber perforated caissons [J]. *Journal of Engineering Mathematics*, 2012, 74: 1-18.

[18] Bhattacharjee J., Soares C. G. Wave interaction with a floating rectangular box near a vertical wall with step type bottom topography [J]. *Journal of Hydrodynamics*, 2010, 22(1): 91-96.

[19] Behera H., Kaligatla R. B., Sahoo T. Wave trapping by porous barrier in the presence of step type bottom [J]. *Wave Motion*, 2015, 57: 219-230.

[20] Koley S., Sahoo T. Oblique wave trapping by vertical permeable membrane barriers located near a wall [J]. *Journal of Marine Science and Application*, 2017, 16(4): 490-501.

[21] Jung T. H., Suh K. D., Lee S. O. et al. Transformation of long waves propagating over trench [J]. *Journal of Korean Society of Coastal and Ocean Engineers*, 2007, 19(3): 228-236.

[22] Roy R., Chakraborty R., Mandal B. N. Propagation of water waves over an asymmetrical rectangular trench [J]. *The Quarterly Journal of Mechanics and Applied Mathematics*, 2016, 70(1): 49-64.